

Interband characterization and electronic transport control of nanoscaled GeTe/Sb₂Te₃ superlattices

Antonio Caretta,^{1,*} Barbara Casarin,^{1,2} Paola Di Pietro,¹ Andrea Perucchi,¹ Stefano Lupi,¹ Valeria Bragaglia,³ Raffaella Calarco,³ Felix Rolf Lutz Lange,⁴ Matthias Wuttig,⁴ Fulvio Parmigiani,^{1,5} and Marco Malvestuto¹

¹*Elettra-Sincrotrone Trieste S.C.p.A. Strada Statale 14 - km 163.5 in AREA Science Park 34149 Basovizza, Trieste, Italy*

²*Università degli Studi di Trieste, Via A. Valerio 2, 34127 Trieste, Italy*

³*Paul-Drude-Institut für Festkörperelektronik, Hausvogteiplatz 5-7, 10117 Berlin, Germany*

⁴*I. Physikalisches Institut (IA), RWTH Aachen University, 52056 Aachen, Germany*

⁵*International Faculty, University of Cologne, 50937 Cologne, Germany*

(Received 28 May 2016; revised manuscript received 7 July 2016; published 28 July 2016)

The extraordinary electronic and optical properties of the crystal-to-amorphous transition in phase-change materials have led to important developments in memory applications. A promising outlook is offered by nanoscaling such phase-change structures. Following this research line, we study the interband optical transmission spectra of nanoscaled GeTe/Sb₂Te₃ chalcogenide superlattice films. We determine, for films with varying stacking sequence and growth methods, the density and scattering time of the free carriers, and the characteristics of the valence-to-conduction transition. It is found that the free carrier density decreases with increasing GeTe content, for sublayer thicknesses below ~ 3 nm. A simple band model analysis suggests that GeTe and Sb₂Te₃ layers mix, forming a standard GeSbTe alloy buffer layer. We show that it is possible to control the electronic transport properties of the films by properly choosing the deposition layer thickness, and we derive a model for arbitrary film stacks.

DOI: [10.1103/PhysRevB.94.045319](https://doi.org/10.1103/PhysRevB.94.045319)

I. INTRODUCTION

Phase-change materials (PCMs) constitute a class of semiconductors characterized by two allotrope phases, a crystalline and an amorphous one, having distinct physical properties [1,2]. Such materials, discovered in the late 1960's [3], are already being used in rewritable optical disks, such as DVDs and Blu-ray disks. They are also very promising to realize fast, nonvolatile electronic memories (PCRAMs). Because of the variety of PCMs, a rigorous chemical definition is absent, although design schemes for some ternary compounds are well established [1,4,5]. A practical requirement for a PCM, as underlined in Ref. [5], is that the switching between the two phases must be reversible, efficient, and repeatable, due to obvious technological reasons. Benchmark PCMs are alloys composed of Ge, Sb, and Te—along the so-called GeTe-Sb₂Te₃ pseudobinary line—thus denoted as GST [6–8]. Although the potential for applications of PCMs spans from dynamic memories [9] to display fabrication [10], at present the limits for the use of GSTs are the speed and the power required to switch between the two phases, being respectively of approximately 100 ns and 100 μ W [11]. Hence, a huge effort is being devoted to finding new solutions, and nanoscale structures seem to offer significant advantages [12]. Following this trend, phase-change heterostructures have been produced, showing to function with improved performances [13]. Here, we focus on chalcogenide superlattice (CSL) films made by high-temperature deposition of alternating nm-sized layers of GeTe and Sb₂Te₃ [14].

Prior to investigating the properties of CSLs, we review the charge carrier transport [15,16] and the structural [17–21] properties of GST compounds. The crystal phase of GSTs is

characterized by a strong dependence of the resistivity upon annealing treatment [15]. In fact, by increasing the temperature, the system undergoes an insulator-metal transition (IMT) at 275 °C, due to disorder reduction [15]. Density functional theory calculations showed that the insulating state is caused by the localization of charge carriers in vacancy-rich areas, and the transition to the metallic state happens when vacancies reconfigure into ordered layers [16]. The presence of vacancy layers in the high-temperature annealed phase of GSTs was proven by high-resolution transmission electron microscopy (TEM) and electron diffraction [22].

The lattice structure of the crystalline Ge-Sb-Te based CSL is similar, by growth design, to the high-temperature GST phase. As mentioned before, CSLs are formed by high-temperature deposition—although lower than the IMT—of GeTe and Sb₂Te₃ layers. One might consequently expect that the as-grown structure is characterized by well separated layers of pure GeTe and Sb₂Te₃. Recent TEM and extended x-ray absorption fine structure (EXAFS) experiments [14,23] have shown that the structure is indeed layered, but GeTe is not actually pure since it is intercalated into a Sb₂Te₃ quintuple layer. Please note that the vacancy layers, when two-dimensionally extended, are labeled van der Waals gaps [24]. The similarity between the high-temperature-annealed GSTs [15] and the CSLs, besides the structure, is corroborated by the measured resistivity of the latter that increases with increasing temperature, suggesting a metallic type conductivity. Nonetheless, it is not obvious whether also the dielectric properties of CSLs are analogous to those of GST compounds [25–28]. For instance, one of the peculiar characteristics of crystalline GST is the high value of the static dielectric constant, which is evidence of resonance bonding [29]. Measuring the dielectric function of CSLs will provide useful information either about the structure, or about the bonding character of the compounds. The dielectric function of CSLs can be estimated

*antonio.caretta@elettra.eu

by transmittance experiments, probing simultaneously the character of the interband transition and the density of free electrons.

In this article we compare the optical transmission behavior of films grown by dc magnetron sputtering (MS), with those grown by molecular beam epitaxy (MBE) used as a reference sample. Transmission experiments are performed on films with thicknesses below 100 nm, to guarantee high film quality, and at normal incidence, to simplify the interpretation of the results. Our analysis supports recent results showing that the GeTe layers are not isolated but intercalated within a Sb₂Te₃ layer [14,23]. We explain how intermixing modifies the conductivity of the film. In addition, we show that it is possible to control the electronic transport properties of the CSL not only by an annealing treatment, as in Ref. [15], but also by means of a specific stack design. In fact, as we will see, the CSL conductivity depends on the layer sequence, giving a different design pathway for the control of the material properties.

II. EXPERIMENT

CSL samples are grown by MS and MBE on Sb-passivated Si(111) surfaces of intrinsic 500- μm -thick wafers above 210 °C. MS samples are films of 15 repetitions of [GeTe(N nm)/Sb₂Te₃(3 nm)], where $N = 1, 2, 3$. For the MBE samples we use the intermediate $N = 2$ case. Growing μm -thick samples is not beneficial for transmittance experiments since stacking defects in the CSL will increase exponentially. MS annealed (ANN) samples—at 250 °C for 30 min—are distinguished from the MS as-deposited (ASD) ones. Transmission experiments in the energy range 0.06–1.23 eV were collected at the SISSI beamline on the Elettra storage ring [30] by a Bruker VERTEX 70v spectrometer. The data range used is 0.075–1 eV due to the fact that, at low energies, the light source intensity is low and, above 1.1 eV, the light is absorbed by the Si substrate (indirect band gap). Please note that it is not possible to use glass transparent substrates in order to improve the transmittance experiments, since the CSLs must be specifically grown on the Si(111) surface to guarantee epitaxy. Furthermore, we used, for each sample, the respective clean substrate as a reference. The fitting function is determined for multilayer thin film optics [31].

III. FITTING MODEL AND RESULTS

Figure 1 shows the absorbance $-\ln(T_{\text{CSL}}/T_{\text{Si}})$, with T_{CSL} and T_{Si} respectively the sample and the substrate transmission, as a function of the incoming photon energy for all the samples. The data present few physically relevant features, common to all samples and regardless of growth technique and layer stack. In particular, we observe (i) the onset of an absorption edge below ~ 0.15 eV, increasing by decreasing the photon energy, (ii) a minimum between 0.15 and 0.3 eV, and (iii) a broad feature rising above ~ 0.4 eV, increasing towards higher energies. In analogy to Ref. [29], we associate the low frequency absorption component to free Drude electrons, and the higher-energy broadband to the onset of the valence-to-conduction absorption. The absorption modulation of the data, particularly visible on the MS 33 annealed sample, is an

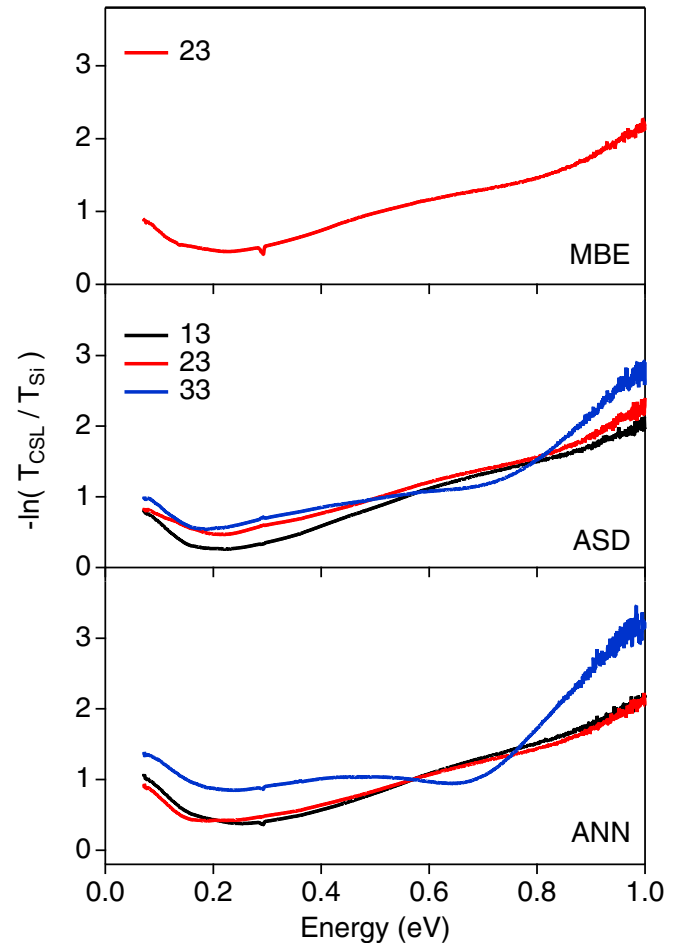


FIG. 1. Absorbance spectra of MBE 23, MS 13-23-33 as-deposited (ASD) and MS 13-23-33 annealed (ANN) samples.

artifact due to multilayer interference effects. We account for interference effects by calculating the transmission coefficient $T_{\text{data}} = T_{\text{CSL}}/T_{\text{Si}}$ including reflection losses.

The film dielectric function (DF) is modeled with a sum of a Drude and a single Tauc-Lorentz (TL) oscillator term [29,32],

$$\epsilon(x) = \epsilon^{\text{Drude}}(x) + \epsilon^{\text{TL}}(x), \quad (1)$$

where

$$\epsilon^{\text{Drude}}(x) = -\frac{\omega_p^2}{x^2 + 1/\tau^2} + i\frac{\omega_p^2}{x\tau(x^2 + 1/\tau^2)},$$

with x the photon energy, ω_p the plasma frequency, and τ the scattering time. The real part of ϵ^{Drude} is a negative Lorentzian function centered at zero while the imaginary part is positive and diverges at zero. The Tauc-Lorentz dielectric function is obtained by Kramers-Kronig integration [$\epsilon_1(x) = 1 + \frac{1}{\pi} \int_{-\infty}^{\infty} \frac{\epsilon_2(x')}{x'-x} dx'$] from the imaginary part,

$$\begin{cases} \epsilon_2^{\text{TL}}(x \leq E_g) & = 0, \\ \epsilon_2^{\text{TL}}(x > E_g) & = \frac{ACE_0(x-E_g)^2}{x[(x^2-E_0^2)^2 + C^2x^2]}, \end{cases} \quad (2)$$

where A is the TL amplitude, E_g is the Tauc—or optical—gap, C is the bandwidth, and E_0 is the central frequency,

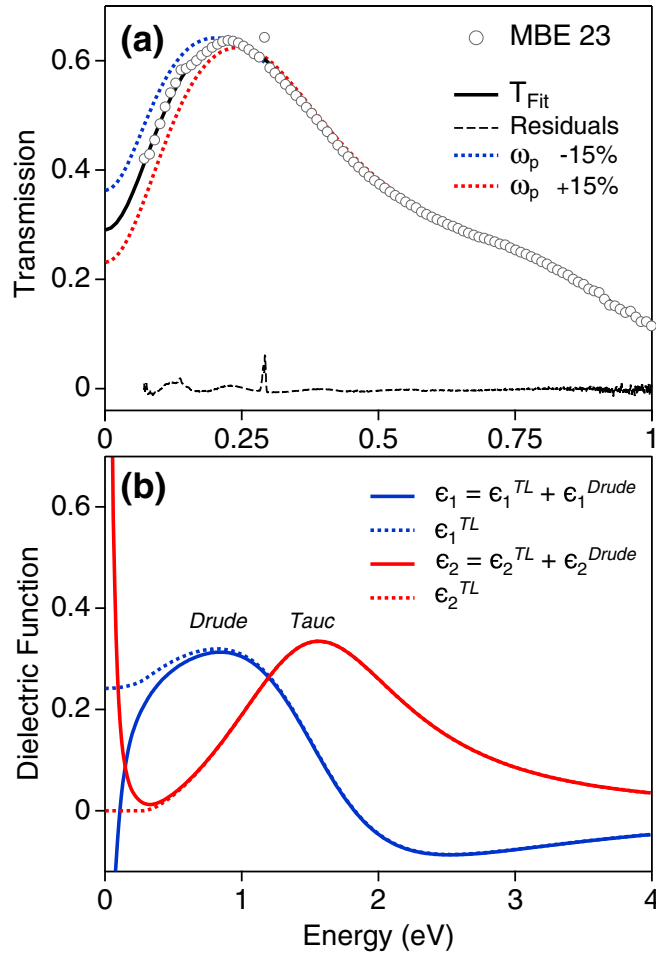


FIG. 2. (a) Transmission data for MBE 23 and fitting curve T_{fit} . The fitting curve is also recalculated for different values of ω_p ($\pm 15\%$). (b) Dielectric function resulting from the fit (please note that the x axis is expanded). Both the real (red) and the imaginary (blue) components of the DF are shown also subtracting the Drude contribution (dashed).

representing the photon energy where the transition probability is at the maximum.

For the (intrinsic) silicon substrate we use $\epsilon(x) \sim 3.45$ [33]. We verified the assumptions made for the dielectric properties of the substrate by transmittance measurements on virgin wafers. Regarding the calculation of $T_{\text{fit}}(x)$, we include multiple coherent propagation only for the thin CSL film. Also, the CSL film thickness is a free parameter of the fitting procedure. A typical fit result is shown in Fig. 2(a). The related DF is plotted in Fig. 2(b). The misfit between the experimental and calculated data is due to Si phonons (the peak at ~ 0.3 eV) and probably to the small contribution of interference effect from the substrate that have not been accounted for. In Fig. 2(a) we also show the transmission curve calculated with different values of ω_p ($\pm 15\%$). Interestingly, although the data points do not cover the full Drude low-energy component of the transmittance, the fit is definitely still accurate, at least within this variation range of ω_p . In all cases the fit function $T_{\text{fit}}(x)$ describes all the main features of the transmission data, thus the deduced parameters are meaningful.

TABLE I. Parameters resulting from the fit of Eq. (1) for all the measured samples. The error on the fit procedure is shown in parentheses, representing the deviation of the last digit. The low-energy limit of the TL DF, $\epsilon_1^{\text{TL}}(0)$, is also computed. *Please note that $1 \text{ eV} = 1.5193 \times 10^{15} \text{ rad/s}$.

	TL			Drude	
	E_g (eV)	E_0 (eV)	$\epsilon_1^{\text{TL}}(0)$	ω_p (eV)*	τ (fs)
MBE 23	0.3(1)	1.7(2)	23	0.7(1)	8(2)
ASD 13	0.1(2)	1.5(2)	35	1.0(1)	9(2)
ASD 23	0.0(1)	1.5(1)	29	0.9(1)	6(2)
ASD 33	0.0(1)	1.5(1)	24	0.7(1)	7(2)
ANN 13	0.1(2)	1.3(1)	30	1.1(1)	8(2)
ANN 23	0.0(1)	1.3(1)	24	0.8(1)	13(2)
ANN 33	0.5(1)	1.5(1)	23	0.7(1)	6(2)

The fit parameters for the TL oscillator and the Drude term, for each investigated CSL, are given in Table I.

IV. DISCUSSION

We first consider the TL component of the DF, whose E_g (eV), E_0 (eV), and $\epsilon_1^{\text{TL}}(0)$ parameters are given in Table I. The Tauc gap lies below 0.5 eV. E_0 , representing the maximum of the semiconductor optical absorption, has an average value of approximately 1.5 eV. This value matches quite well with the experimentally obtained value of crystalline GeTe [34] and GST [29]. Moreover, the computed low frequency value of the real part of the TL DF, $\epsilon_1^{\text{TL}}(0)$, has an average value above 20. This high $\epsilon_1^{\text{TL}}(0)$ value is typical of the crystal phase of PCMs [29], suggesting the presence of resonance bondings. In summary, the TL component of our CSL is approximately independent on the annealing treatment. The fact that annealing does not affect the as-deposited (ASD) structures might suggest that the films undergo an immediate reorganization during growth, which is more effective than annealing itself [35]. The analysis of the free electrons in our CSL supports this hypothesis.

The plasma frequency and the scattering time, resulting from the fitting procedure, are presented in Table I. While the scattering time ranges between 5 and 15 fs—just half with respect to Copper at 300 K [36]—the plasma frequency consistently decreases with the increase of the stacking sequence 13-23-33, both for the ASD and ANN samples. The CSL carrier density $n = \frac{m_e \epsilon_0}{e^2} \omega_p^2$, derived from ω_p with the vacuum permittivity ϵ_0 , and m_e and e respectively the electron mass and charge, is shown in Fig. 3. A decrease of n is observed with the increase of nominal GeTe content in the film. In general, crystalline GST compounds are p -type semiconductors [37]. At present, the carrier charge and effective mass in CSLs are not known, but this lack of information does not affect the general conclusions reached here. Also, the conductivity $\sigma = \frac{e^2}{m_e} n \tau$ shows the same trend. This behavior can be explained either by an increased defectivity, by a lower conductivity of GeTe with respect to Sb_2Te_3 , or by an increase of the optical gap. Yet, since the comparison acts within the MS grown samples, we expect the same growth quality

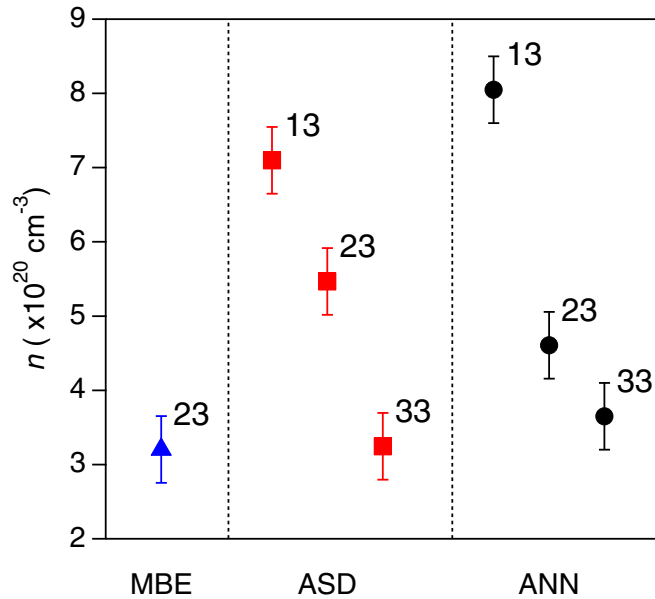


FIG. 3. Free carrier density $n = \frac{m_e \epsilon_0}{e^2} \omega_p^2$ obtained from the Drude term of the fit. A decrease of n is observed with increasing GeTe content.

and—consequently—the same concentration of defects. In addition, pure GeTe has a *higher* free carrier concentration with respect to Sb_2Te_3 [38,39]. Thus, the expected trend with stack sequence 13-23-33 should be opposite than that observed. It follows that variations of n must result from changes of the electronic band structure.

The intermixing of GeTe and Sb_2Te_3 layers raises the material optical gap, causing a reduction of the free carrier concentration. Figure 4(a) sketches the band diagrams for GeTe, Sb_2Te_3 , and GSTs, in analogy to Refs. [15,17]. The diagrams emphasize the differences between the optical gaps and the presence of degenerate electrons in the conduction band. Both GeTe and Sb_2Te_3 have a low Tauc gap, $E_g \sim 0.1$ eV [40–42], while for GST, $E_g^{\text{GST}} \sim 0.4$ eV [29,37,43]. In first approximation the Tauc gap of the CSL depends on the constituents' volume fraction and on their respective gaps. If GeTe and Sb_2Te_3 are ideally separated inside the CSL, the film is expected to have a small gap and high carrier concentration, independent of the relative content of the two elements. If instead GST is formed by the intermixing of the two, the material Tauc gap must rise. The more GST is formed, the higher is the Tauc gap (approaching eventually the value of GSTs) and the lower is the number of degenerate electrons. This is consistent with the carrier density of the sequence 13-23-33, shown in Fig. 3.

V. ELECTRIC TRANSPORT CONTROL

We extrapolate the trend observed in the present CSL to a stack of general thickness, having $(\text{GeTe})_N/(\text{Sb}_2\text{Te}_3)_M$ as a repeat unit, where $N, M \geq 1$. This formula is applicable to all CSL structures developed so far in the literature: (i) superlattice-like (SSL) PCMs, with $N, M > 2$ [44]; (ii) interfacial phase change materials (IPCMs), with $N \leq 4, M \leq 2$ [13]; (iii) the case $N = 2M$, studied in Ref. [39]; and (iv) our CSLs.

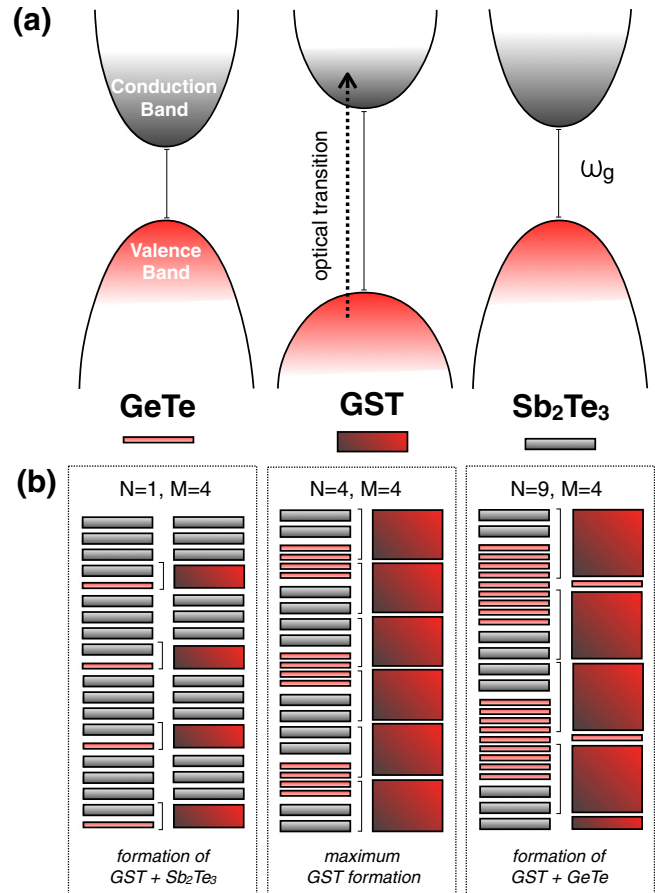


FIG. 4. (a) Sketch of the band diagram of GeTe, Sb_2Te_3 , and GST materials. The Tauc gap E_g in both GeTe and Sb_2Te_3 is lower with respect to GST compounds. Thermal promotion of valence band (VB) electrons to the conduction band (CB) is accordingly reduced in GSTs, hence the free carrier density and the conductivity are lower. (b) Examples of the formation of GST at the interface between GeTe and Sb_2Te_3 ($N = 1, 4, 9$ and $M = 4$, in order from left to right): (i) The formation of a single GST layer leaves three pure Sb_2Te_3 layers; (ii) diffusion involves at most two Sb_2Te_3 and four GeTe layers at each interface, forming a maximum possible GST; (iii) the formation of GST leaves a single pure GeTe layer.

We assume our stack sequence corresponds to $N = 2, 4, 6$ and $M = 3$, since 1 nm of GeTe along the (111) direction is composed of at least two bilayers [14,45]. The conductivity of a CSL in the general case is calculated assuming that GeTe and Sb_2Te_3 layers intermix at the interface, forming GST, as shown in Fig. 4(b). The structure of the intermixed stack is calculated with the following assumptions: (i) It is only possible to form either $\text{Ge}_1\text{Sb}_2\text{Te}_4$ (GST124), or $\text{Ge}_2\text{Sb}_2\text{Te}_5$ (GST225), or $\text{Ge}_3\text{Sb}_2\text{Te}_6$ (GST326); (ii) interdiffusion effects do not involve more than two Sb_2Te_3 and four GeTe layers for each interface; and (iii) among various possible stacking sequences, the one with the highest GST content is chosen for simplicity. The first and second assumptions are motivated by TEM and EXAFS experiments [14,23] on the same CSLs, and by the fact that GST124, GST225, and GST326 are the most stable and favorable GST structures [22]. All these assumptions could be refined but, as we report below, they

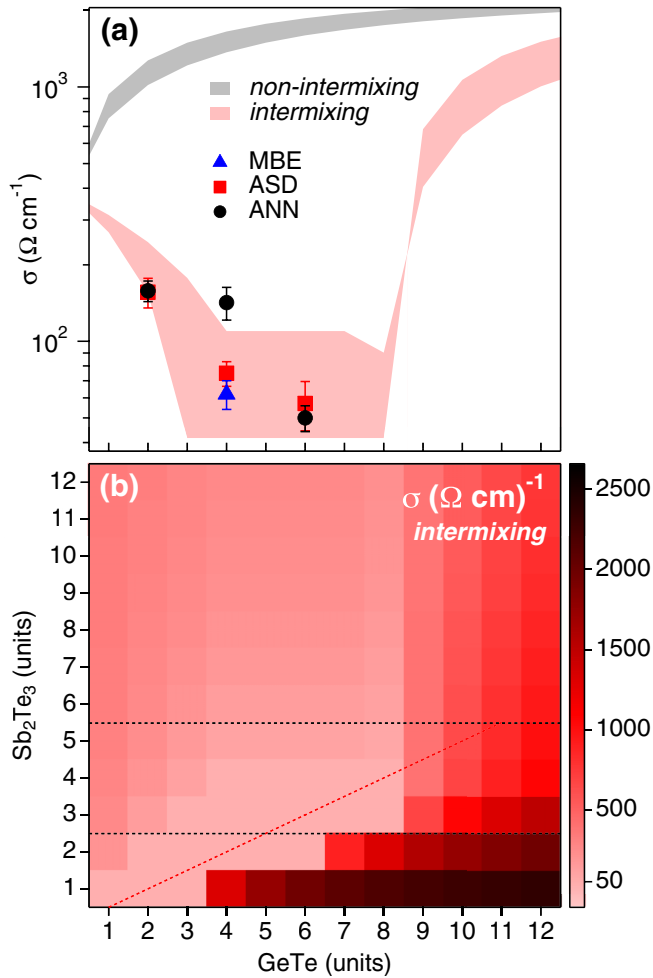


FIG. 5. (a) Conductivity of the film calculated from Eq. (3) for an increasing number of GeTe units, and compared with the measured conductivity of the CSLs. (b) Conductivity of a film with stack sequence $(\text{GeTe})_N/(\text{Sb}_2\text{Te}_3)_M$. The red dashed diagonal indicates the lowest conductivity region. The black dashed horizontal lines represent the cut used to generate (a).

are sufficient to properly describe the experimental trends. We also include a few examples in Fig. 4(b) in order to clarify the model. Given the bulk conductivities σ_{GeTe} , $\sigma_{\text{Sb}_2\text{Te}_3}$, and σ_{GST} [39], the film conductivity is finally calculated as

$$\sigma^{(N,M)} = \sum_i v_i \sigma_i, \quad (3)$$

where v_i is the volume fraction of the i th component (GeTe, Sb_2Te_3 , and GST).

In Fig. 5(a), the conductivity measured for all our samples is compared with the conductivity $\sigma^{(N,M=3)}$, as a function of GeTe layer units N . In agreement with experimental observations, the conductivity decreases from $N = 1$ down to $N \sim 8$. The strikingly different behavior of the “nonintermixing” case, calculated simply via Eq. (3) with $v_{\text{GST}} = 0$, demonstrates once more that intermixing effects must be accounted for when working with superlattice structures.

For completeness, the dependence of $\sigma^{(N,M)}$ is shown in Fig. 5(b). It is interesting to note that the conductivity has a minimum along the diagonal $M \sim N/2$ up to $N = 8$ that corresponds to the maximum possible volumetric formation of GST, hence forming the material with the lowest conductivity. For higher values of N and M , the conductivity approaches the “nonintermixing” case, as also visible for high values of the GeTe units in Fig. 5(a). We want to underline that intermixing effects were most probably already present in Ref. [39], where the case $M = N/2$ (equal sublayer thickness) was studied. These authors, in fact, observe that the superlattice films always have lower conductivity with respect to GeTe and Sb_2Te_3 , in agreement with our picture.

VI. CONCLUSION

In this work we deduce important structural details of crystalline GeTe/ Sb_2Te_3 superlattice deposited at high temperature ($>210^\circ\text{C}$) by studying the film interband transmission. We observe that, at the interface between the GeTe and Sb_2Te_3 deposition layers, a crystalline GST compound is already formed during growth. GST, having a higher band gap with respect to its constituents, lowers the number of degenerate conduction electrons. By varying the respective number of building block layers it is possible to control the percent of GST in the film, and consequently the film conductivity, with no need of an annealing treatment. In the future it would be interesting to investigate the dynamics deriving from the intermixing and ion diffusion by depositing two single thick layers of GeTe and Sb_2Te_3 and studying the interface effects at different deposition and annealing conditions.

ACKNOWLEDGMENTS

This work was supported by EU within FP7 project PASTRY (GA 317764). A.C. would like to acknowledge Roberta Ciprian for useful comments.

- [1] D. Lencer, M. Salinga, and M. Wuttig, *Adv. Mater.* **23**, 2030 (2011).
- [2] V. L. Deringer, R. Dronskowski, and M. Wuttig, *Adv. Funct. Mater.* **25**, 6343 (2015).
- [3] S. R. Ovshinsky, *Phys. Rev. Lett.* **21**, 1450 (1968).
- [4] N. Mott and E. Davis, *Electronic Processes in Non-Crystalline Materials* (Oxford University Press, Oxford, UK, 1971).
- [5] D. Lencer, M. Salinga, B. Grabowski, T. Hickel, J. Neugebauer, and M. Wuttig, *Nat. Mater.* **7**, 972 (2008).
- [6] M. Chen, K. A. Rubin, and R. W. Barton, *Appl. Phys. Lett.* **49**, 502 (1986).
- [7] N. Yamada, E. Ohno, K. Nishiuchi, N. Akahira, and M. Takao, *J. Appl. Phys.* **69**, 2849 (1991).
- [8] M. Wuttig and N. Yamada, *Nat. Mater.* **6**, 824 (2007).
- [9] M. Wuttig, *Nat. Mater.* **4**, 265 (2005).
- [10] P. Hosseini, C. D. Wright, and H. Bhaskaran, *Nature (London)* **511**, 206 (2014).

- [11] B. C. Lee, E. Ipek, O. Mutlu, and D. Burger, *ACM SIGARCH Comput. Archit. News* **37**, 2 (2009).
- [12] M. H. R. Lankhorst, B. W. S. M. M. Ketelaars, and R. A. M. Wolters, *Nat. Mater.* **4**, 347 (2005).
- [13] R. E. Simpson, P. Fons, A. V. Kolobov, T. Fukaya, M. Krbal, T. Yagi, and J. Tominaga, *Nat. Nanotechnol.* **6**, 501 (2011).
- [14] J. Momand, R. Wang, J. E. Boschker, M. A. Verheijen, R. Calarco, and B. J. Kooi, *Nanoscale* **7**, 19136 (2015).
- [15] T. Siegrist, P. Jost, H. Volker, M. Woda, P. Merkelbach, C. Schlockermann, and M. Wuttig, *Nat. Mater.* **10**, 202 (2011).
- [16] W. Zhang, A. Thiess, P. Zalden, R. Zeller, P. H. Dederichs, J.-Y. Raty, M. Wuttig, S. Blügel, and R. Mazzarello, *Nat. Mater.* **11**, 952 (2012).
- [17] M. H. Cohen, H. Fritzsche, and S. R. Ovshinsky, *Phys. Rev. Lett.* **22**, 1065 (1969).
- [18] A. V. Kolobov, P. Fons, A. I. Frenkel, A. L. Ankudinov, J. Tominaga, and T. Uruga, *Nat. Mater.* **3**, 703 (2004).
- [19] J. Akola and R. O. Jones, *Phys. Rev. B* **76**, 235201 (2007).
- [20] A. V. Kolobov, M. Krbal, P. Fons, J. Tominaga, and T. Uruga, *Nat. Chem.* **3**, 311 (2011).
- [21] P. Jost, H. Volker, A. Poitz, C. Poltorak, P. Zalden, T. Schfer, F. R. L. Lange, R. M. Schmidt, B. Hollnder, M. R. Wirtsohn, and M. Wuttig, *Adv. Funct. Mater.* **25**, 6399 (2015).
- [22] B. J. Kooi and J. T. M. De Hosson, *J. Appl. Phys.* **92**, 3584 (2002).
- [23] B. Casarin, A. Caretta, J. Momand, B. J. Kooi, M. A. Verheijen, V. Bragaglia, R. Calarco, M. Chukalina, X. Yu, J. Robertson, F. R. L. Lange, M. Wuttig, A. Redaelli, E. Varesi, F. Parmigiani, and M. Malvestuto, *Sci. Rep.* **6**, 22353 (2016).
- [24] O. Oeckler, in *Minerals as Advanced Materials II*, edited by V. S. Krivovichev (Springer, Berlin, 2012), pp. 333–340.
- [25] G. Lucovsky and R. M. White, *Phys. Rev. B* **8**, 660 (1973).
- [26] P. B. Littlewood, *J. Phys. C* **12**, 4459 (1979).
- [27] R. Yokota, *Jpn. J. Appl. Phys.* **28**, 1407 (1989).
- [28] B. Huang and J. Robertson, *Phys. Rev. B* **81**, 081204 (2010).
- [29] K. Shportko, S. Kremers, M. Woda, D. Lencer, J. Robertson, and M. Wuttig, *Nat. Mater.* **7**, 653 (2008).
- [30] S. Lupi, A. Nucara, A. Perucchi, P. Calvani, M. Ortolani, L. Quaroni, and M. Kiskinova, *J. Opt. Soc. Am. B* **24**, 959 (2007).
- [31] S. J. Byrnes, *arXiv:1603.02720*.
- [32] G. E. Jellison, Jr. and F. A. Modine, *Appl. Phys. Lett.* **69**, 371 (1996).
- [33] <http://refractiveindex.info>.
- [34] A. Velea, G. Socol, M. Popescu, and A. C. Galca, *J. Appl. Phys.* **118**, 135712 (2015).
- [35] R. Wang, V. Bragaglia, J. E. Boschker, and R. Calarco, *Cryst. Growth Des.* **16**, 3596 (2016).
- [36] G. L. Eesley, *Phys. Rev. B* **33**, 2144 (1986).
- [37] T. Kato and K. Tanaka, *Jpn. J. Appl. Phys.* **44**, 7340 (2005).
- [38] J. M. Yáñez-Limón, J. González-Hernández, J. J. Alvarado-Gil, I. Delgadillo, and H. Vargas, *Phys. Rev. B* **52**, 16321 (1995).
- [39] H. Tong, N. N. Yu, Z. Yang, X. M. Cheng, and X. S. Miao, *J. Appl. Phys.* **118**, 075704 (2015).
- [40] R. Tsu, W. E. Howard, and L. Esaki, *Phys. Rev.* **172**, 779 (1968).
- [41] S. K. Bahl and K. L. Chopra, *J. Appl. Phys.* **40**, 4940 (1969).
- [42] M. M. Ibrahim, M. M. Wakkad, E. K. Shokr, and H. A. Abd El-Ghani, *Appl. Phys. A* **52**, 237 (1991).
- [43] J.-W. Park, S. H. Baek, T. D. Kang, H. Lee, Y.-S. Kang, T.-Y. Lee, D.-S. Suh, K. J. Kim, C. K. Kim, Y. H. Khang, J. L. F. Da Silva, and S.-H. Wei, *Appl. Phys. Lett.* **93**, 021914 (2008).
- [44] T. C. Chong, L. P. Shi, R. Zhao, P. K. Tan, J. M. Li, H. K. Lee, X. S. Miao, A. Y. Du, and C. H. Tung, *Appl. Phys. Lett.* **88**, 122114 (2006).
- [45] J. Tominaga, A. V. Kolobov, P. Fons, T. Nakano, and S. Murakami, *Adv. Mater. Interfaces* **1**, 1300027 (2013).